Supporting information

Incorporation of Rubidium Cations into Blue Perovskite Quantum Dots Light-Emitting Diodes via FABr Modified Multication Hot-Injection Method

Fanyuan Meng, Xinyan Liu, Xinyi Cai, Zifeng Gong, Binbin Li, Wentao Xie, Mengke Li, Dongcheng Chen*, Hin-Lap Yip, Shi-Jian Su*

State Key Laboratory of Luminescent Materials and Devices and Institute of Polymer Optoelectronic Materials and Devices, South China University of Technology, Guangzhou 510640, China

E-mail: mssjsu@scut.edu.cn, mschendc@scut.edu.cn

Keywords: rubidium cation, perovskite quantum dots, photoluminescence quantum yield, exciton binding energy, blue perovskite light-emitting diodes

Experimental Section

Materials. Lead chloride ($PbCl_2$, 99.5%, Xi'an p-OLED Corp), lead bromide ($PbBr_2$, 99.5%, Xi'an p-OLED Corp), formamidinium bromide (FABr, 99.5%, Xi'an p-OLED Corp), cesium carbonate (Cs_2CO_3, 99.995%, Aldrich), rubidium carbonate (Rb_2CO_3, 99.994%, Alfa), octadecene (90%, alfa), oleylamine (90%, innochem), oleic acid (90%, alfa), and ethyl acetate (99.9%, aladdin) were used as received without further purification.

Synthesis of Cs-oleate. Cs-oleate was prepared by adding Cs_2CO_3 (0.4 g) into a three-necked flask with octadecene (15 mL) and oleic acid (1.23 mL). The mixture was dried at 120 °C under an argon (Ar) atmosphere for 1.5 h, and then heated to 150 °C for 1 h.

Synthesis of Rb-oleate. Rb-oleate was prepared by loading Rb_2CO_3 (0.283 g) into a three-necked flask with octadecene (15 mL) and oleic acid (1.3 mL). The mixture was dried at 120 °C under an Ar atmosphere for 1.5 h, and then heated to 170 °C for 1 h.

Synthesis of perovskite QDs with traditional hot-injection method. For $CsPbBr_3$ QD, $PbBr_2$ (0.2 g) was added into a 100 mL three-necked flask with octadecene (15 mL), oleylamine (3.0 mL) and oleic acid (1.5 mL). The mixture was dried at 120 °C under an Ar atmosphere for 1.0 h and then heated at 170 °C for 10 min. After that, 0.55 mL Cs-oleate was quickly injected into the three-necked flask. After 5 s, the reaction was terminated with ice-water bath. The crude solution was washed with ethyl acetate via centrifugation and dispersed in octane for further characterization and device fabrication. For $Rb_{0.33}Cs_{0.67}PbBr_3$ QD, 0.55 mL Cs-oleate was replaced by 0.55 mL mixed-oleate (Rb:Cs=1:2) with other conditions remain unchanged. For $(Rb_{0.33}Cs_{0.67})_{0.42}FA_{0.58}PbBr_3$ (À-QD), 0.55 mL Cs-oleate was replaced by 0.55 mL mixed-oleate (Rb:Cs:FA=0.33:0.67:1.37) with other conditions remain unchanged.

Synthesis of perovskite QDs with FMMHI method. For $(Rb_{0.33}Cs_{0.67})_{0.42}FA_{0.58}PbBr_3$ (A-QD) prepared with FMMHI method, $PbBr_2$ (0.2 g) and FABr (0.094 g) was added into a 100 mL three-necked flask with octadecene (15 mL), oleylamine (3.0 mL) and oleic acid (1.5 mL). The mixture was dried at 120 °C under an Ar atmosphere for 1.0 h and then heated at 170 °C for 10 min. Then 0.55 mL mixed-oleate (Rb:Cs=1:2) was quickly injected into the three-necked flask. After 5 s, the reaction was terminated with ice-water bath. The crude solution was washed with ethyl acetate via centrifugation and dispersed in octane for further characterization and device fabrication. For $(Rb_{0.33}Cs_{0.67})_{0.42}FA_{0.58}PbCl_{1.25}Br_{1.75}$ (B-QD), $PbBr_2$ (0.2 g) was replaced by $PbBr_2$ (0.117 g) and $PbCl_2$ (0.087 g) with other conditions remain unchanged. For $Cs_{0.42}FA_{0.58}PbBr_3$ QD, 0.55 mL mixed-oleate (Rb:Cs=1:2) was replaced by Cs-oleate (0.55 mL) with other conditions remain unchanged. For $(Rb_{0.33}Cs_{0.67})_{0.55}FA_{0.55}PbBr_3$ QD, FABr (0.094 g) was replaced by FABr (0.068 g) with other conditions remain unchanged. For $(Rb_{0.33}Cs_{0.67})_{0.33}FA_{0.67}PbBr_3$ QD, FABr (0.094 g) was replaced by FABr (0.136 g) with other conditions remain unchanged.

Device Fabrication and Characterization. The devices were fabricated following a well-established procedure. First, ITO substrates were carefully cleaned by acetone, isopropyl alcohol, detergent, deionized water, and isopropyl alcohol under ultrasonic bath and treated with O_2 plasma for 10 min in sequence. After a 30 nm thin film of poly-TPD was spin-coated from its chlorobenzene solution and then baked at 110 °C for 10 min. Then a 30 nm thin film of perovskite QD emitters was spin-coated from octane solution. The thickness of poly-TPD and emitting layers was determined by a profiler, Tencor Alfa-Step 500. Finally, 50 nm of TPBI, 4 nm of Ba, and 120 nm of aluminium were evaporated with a shadow mask at a base pressure of 1×10^{-4} Pa. The thickness of the evaporated ETL and cathode was monitored by a quartz crystal thickness monitor (Model: STM-100/MF, Sycon). The overlapping area between the cathode and anode defined the emission area as a pixel size of 15 mm^2. All of the fabrication processes were carried out inside a controlled atmosphere of nitrogen dry-box containing less than 1 ppm oxygen and moisture. Current density (J)-luminance (L)-voltage (V) characteristics were collected using a Keithley 236 source meter and a calibrated silicon photodiode. EL spectra and CIE coordinates were recorded using Ocean Optics USB 2000. EQEs of the devices were calculated from the current density, luminance, and EL spectrum, assuming a Lambertian distribution. Before measured in atmosphere, all the devices were encapsulated with a UV-cured epoxy resin.

Measurement and Characterization. Powder X-ray diffraction (XRD) spectra were taken with a multipurpose XRD system Germen Bruker D8 advance. Scanning electron microscopy (SEM) images were taken with a JEOL JSM-7500F system. High-resolution transmission electron microscopy (HR-TEM) images were recorded on JEM-2100F Field Emission Transmission Electron Microscope. UV-vis absorption spectra were recorded on a HP 8453 spectrophotometer. Photoluminescence (PL) spectra and photostability were measured using a Jobin-Yvon spectrofluorometer. Transient PL decay of perovskite QDs in solid film was measured with an Edinburgh FL920 fluorescence spectrophotometer with a 365 nm laser as the excitation light source. Photoluminescence quantum yields (PLQYs) of perovskite QD films were measured utilizing an integrating sphere of Hamamatsu absolute PL quantum yield spectrometer (C11347-01). Temperature dependent photoluminescence spectra were measured at Ocean Optics fiber spectrometer (QE-pro) with a laser excitation (355 nm) at different temperatures in a closed-circuit liquid nitrogen system. Fourier transform infrared spectroscopy was recorded using a Nicolet 6700 FTIR spectrometer. XPS analysis were measured in an Axis Ultra DLD (Kratos) spectrometer equipped with a mono Al K α X-ray source (E = 1486.6 eV, 5 mA×15 KV) using an aperture slot of 700 µm × 300 µm. GIWAXS measurements were accomplished by MetalJet-D2 X-ray Source (Excillum). The incidence angle of X-ray beam was set to be 0.2° for perovskite QD films. GIWAXS patterns were recorded with a Pilatus3R 1M detector (Dectris). Samples for GIWAXS measurements were prepared by spin-coating perovskite QD solution on silicon substrates. Powder EPMA-EDS analysis was performed by SHIMADZU EPMA-1600 with EDAX-Genesis.

Time-resolved transient photoluminescence decay spectra. Radiative (k_r) and non-radiative transition rate (k_{nr}) of the perovskite QDs with different compositions were calculated following the Equation (S1) and (S2) below:

$$k_r = \Phi / t_{ave} \quad \text{(S1)}$$

$$k_{nr} = 1/ t_{ave} - k_r \quad \text{(S2)}$$

where Φ represents PLQY, t_{ave} represents average lifetime. All data are shown in Table 2.

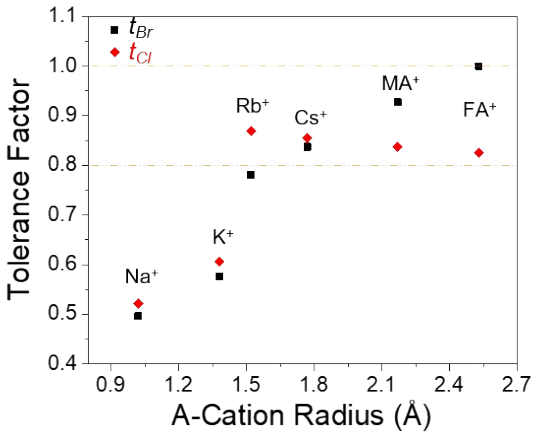

Figure S1. The calculated tolerance factors (t) of $APbX_3$ (A = Na, K, Rb, Cs, MA, FA; X = Cl, Br) QDs as a function of the A-site cation radius. The yellow dashed lines represent the upper and bottom limit of the empirical formability range of the tolerance factors (0.8-1.0).

To select appropriate monovalent cations as the candidate for highly efficient blue perovskite QDs, we calculated the tolerance factors of A-site cations widely used in perovskite solar cells and light-emitting diodes (Figure S1). Rb^+ has a tolerance factor of 0.78 which is very close to the bottom limit value. Thus, we use a mixing strategy where small cations (Rb^+) are added to larger cations (Cs^+ and FA^+) aiming for a stable perovskite structure.

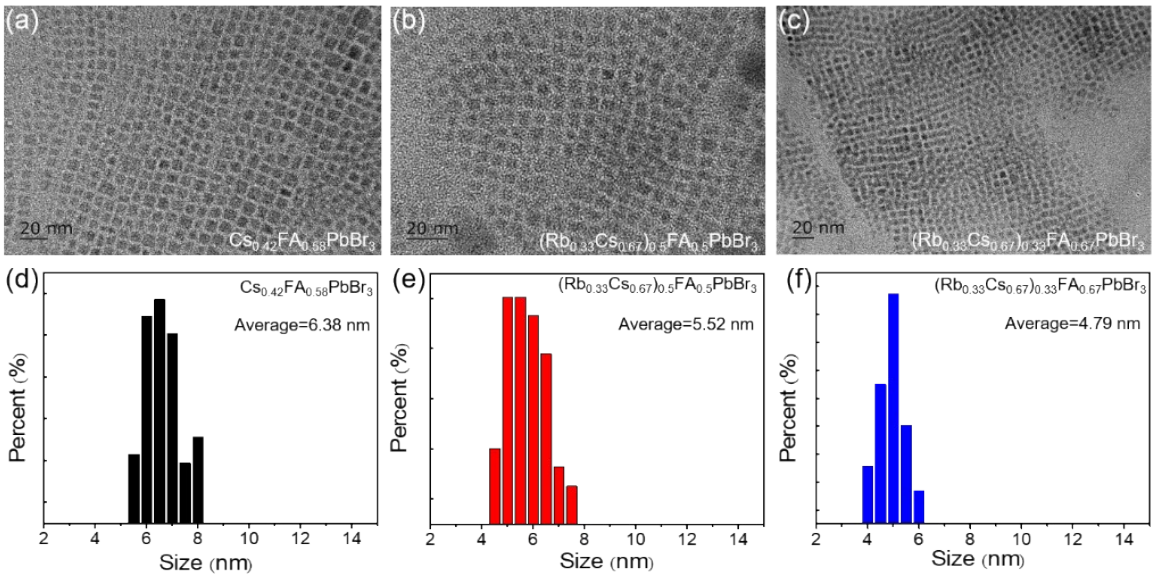

Figure S2. (a), (b), (c) TEM images, and (d), (e), (f) size distributions of the $Cs_{0.42}FA_{0.58}PbBr_3$, $(Rb_{0.33}Cs_{0.67})_{0.5}FA_{0.5}PbBr_3$, and $(Rb_{0.33}Cs_{0.67})_{0.33}FA_{0.67}PbBr_3$ QDs, respectively. The particle sizes were determined by individually measuring the nanocrystal sizes on the TEM images.

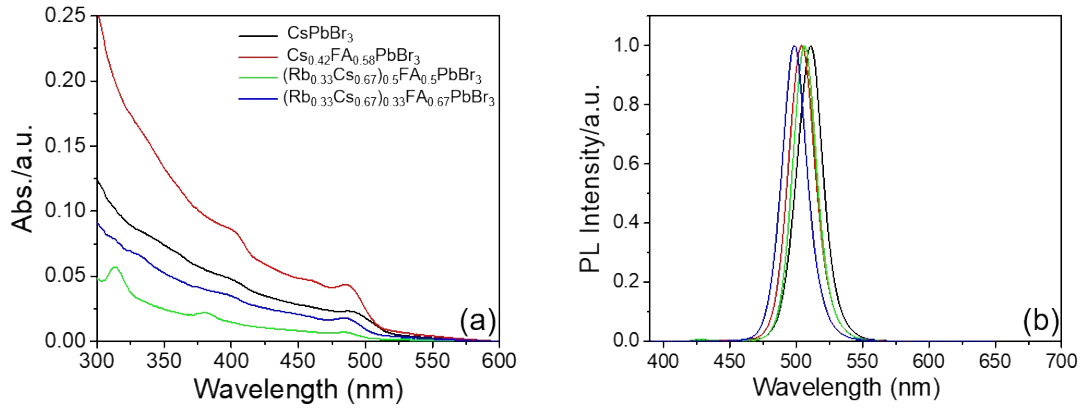

Figure S3. (a) UV-vis absorption and (b) PL spectra of the prepared perovskite QDs with different compositions at room temperature.

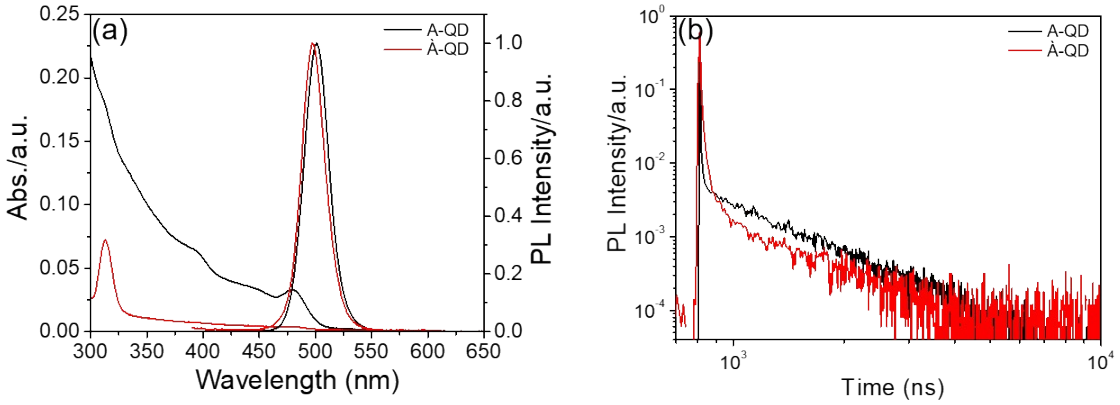

Figure S4. (a) UV-vis absorption and PL spectra, and (b) time-resolved PL decay curves of A-QD and À-QD at room temperature.

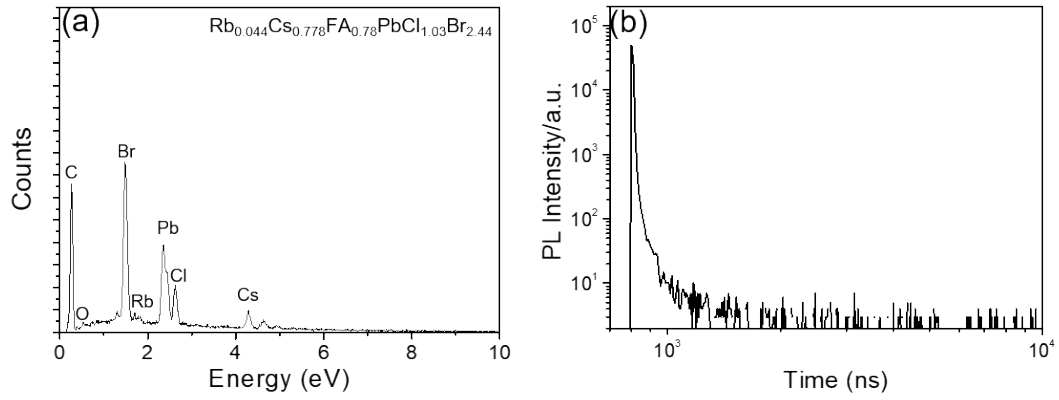

Figure S5. (a) EPMA-EDS spectrum (inset: the actual elemental composition) and (b) time-resolved PL decay curve of the $(Rb_{0.33}Cs_{0.67})_{0.42}FA_{0.58}PbCl_{1.25}Br_{1.75}$ QD.

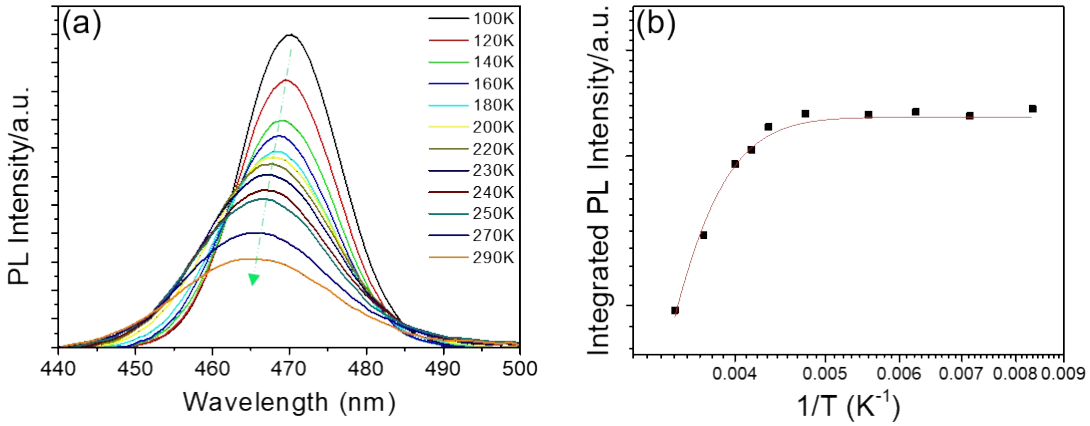

Figure S6. (a) Temperature-dependent PL spectra of the $(Rb_{0.33}Cs_{0.67})_{0.42}FA_{0.58}PbCl_{1.25}Br_{1.75}$ QD taken from 100 to 290 K. (b) Integrated PL intensity of the $(Rb_{0.33}Cs_{0.67})_{0.42}FA_{0.58}PbCl_{1.25}Br_{1.75}$ QD *vs* reciprocal temperature (1/T) from 100 to 290 K.

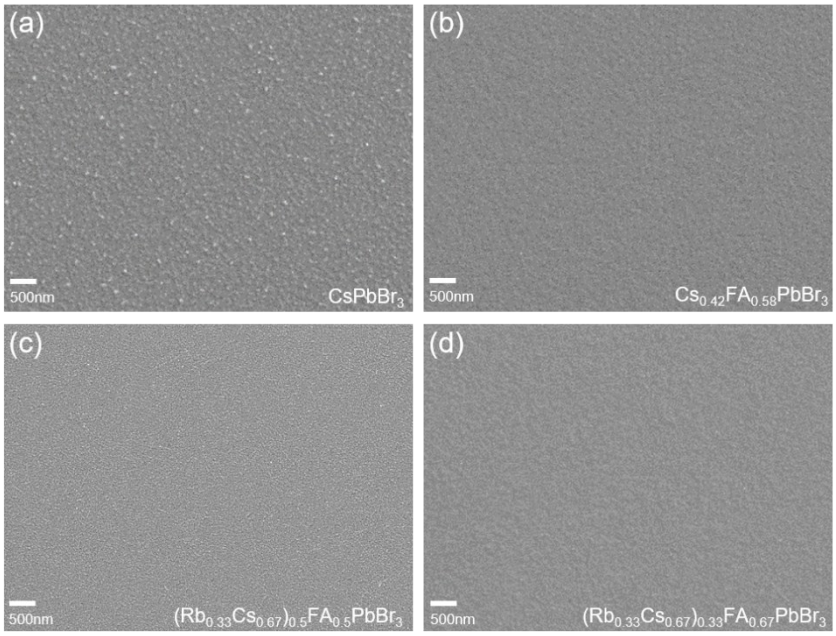

Figure S7. Top view SEM images of the perovskite QD films prepared with different compositions.

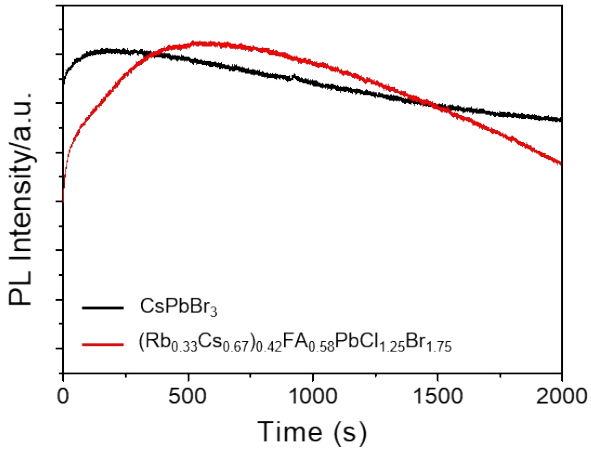

Figure S8. Photostability of different thin films under continuous irradiation at 355 nm from a xenon lamp.

Up to now, the stability of perovskite QDs is still a big challenge, especially for blue QDs. The stability of blue perovskite emitters is generally poor[1] and corresponding data was scarcely reported. To probe the stability of the developed QDs, we performed the photostability measurement upon optical excitation. Photostabilities of deep-blue $(Rb_{0.33}Cs_{0.67})_{0.42}FA_{0.58}PbCl_{1.25}Br_{1.75}$ QDs and $CsPbBr_3$ QDs films were tested under continuous illumination with a 355 nm xenon lamp (52 μW/cm^2) in atmospheric environment (26 °C and humidity of 82%). The PL intensity showed obvious enhancement at the early times for both samples. This phenomenon can be explained by the fact that UV light illumination can cure the surface defect sites.[2,3,4,5] With a continuous light irradiation, the deep-blue $(Rb_{0.33}Cs_{0.67})_{0.42}FA_{0.58}PbCl_{1.25}Br_{1.75}$ QDs film tends to give a quicker decline suggesting lower photostability than $CsPbBr_3$ QDs. Further studies on this issue are still needed in the future.

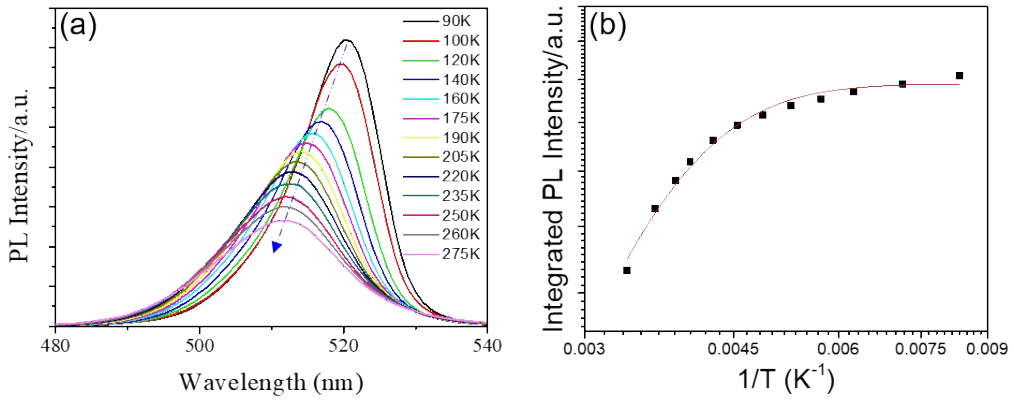

Figure S9. (a) Temperature-dependent PL spectra of the $CsPbBr_3$ QD taken from 90 to 275 K. (b) Integrated PL intensity of the $CsPbBr_3$ QD *vs* reciprocal temperature (1/T) from 90 to 275 K.

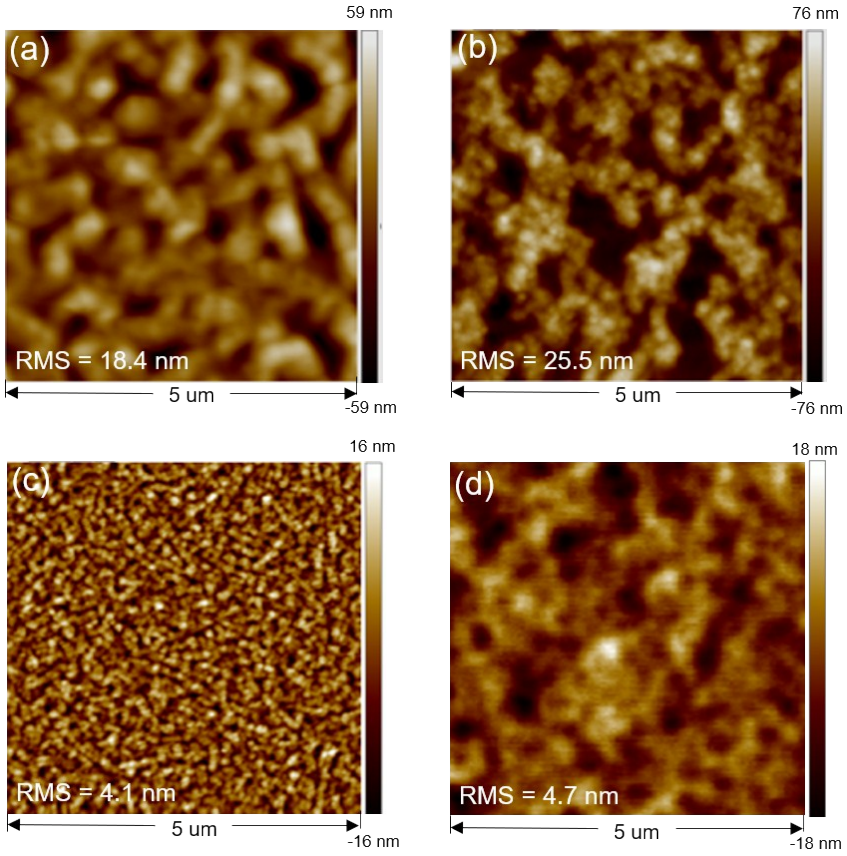

Figure S10. AFM images of the (a) $CsPbBr_3$, (b) $Rb_{0.33}Cs_{0.67}PbBr_3$, (c) $(Rb_{0.33}Cs_{0.67})_{0.42}FA_{0.58}PbBr_3$, and (d) $(Rb_{0.33}Cs_{0.67})_{0.42}FA_{0.58}PbCl_{1.25}Br_{1.75}$ perovskite QDs film, respectively.

Table S1**.** Summary of the room temperature optical properties of the perovskite QD films with different compositions.

Materials	λ_{Abs} (nm)	λ_{PL} (nm)	Energy gap (eV)	FWHM (nm)	PLQY (%)
$CsPbBr_3$	486	511	2.39	23	66.0
$Cs_{0.42}FA_{0.58}PbBr_3$	403, 485	504	2.43	23	67.3
$(Rb_{0.33}Cs_{0.67})_{0.5}FA_{0.5}PbBr_3$	313, 380, 485	506	2.46	23	55.2
$(Rb_{0.33}Cs_{0.67})_{0.33}FA_{0.67}PbBr_3$	484	498	2.49	21	62.7

Table S2. Summary of the room temperature optical properties and PL lifetimes of the perovskite QD films prepared with different methods.

Materials	λ_{Abs} (nm)	λ_{PL} (nm)	FWHM (nm)	PLQY (%)	$\tau 1$ (ns)	$f1$ (%)	$\tau 2$ (ns)	$f2$ (%)	$\tau 3$ (ns)	$f3$ (%)	χ^2	τ_{avg} (ns)	k_r ($10^7 s^{-1}$)	k_{nr} ($10^7 s^{-1}$)	$k_r:k_{nr}$
A-QD	480	500	24	64.5	3.19	93.9	160.9	1.5	803.1	4.7	0.76	42.90	1.46	0.87	1.68
À-QD	313, 477	497	24	23.8	4.75	87.7	26.8	6.9	751.4	5.4	1.14	46.34	0.42	1.74	0.24

Table S3. Powder EPMA-EDS elemental analysis of the perovskite QDs with different compositions.

Materials \ At%	Cs	Rb	C	Pb	Br	Cl	O
$CsPbBr_3$	3.67	-	79.4	3.46	12.23	-	1.24
$Cs_{0.42}FA_{0.58}PbBr_3$	1.96	-	86.49	2.24	7.9	-	0.78
$Rb_{0.33}Cs_{0.67}PbBr_3$	4.77	2.42	73.7	3.05	15.08	-	0.97
$(Rb_{0.33}Cs_{0.67})_{0.42}FA_{0.58}PbBr_3$	2.48	0.24	82.33	2.97	10.56	-	0.87
$(Rb_{0.33}Cs_{0.67})_{0.42}FA_{0.58}PbCl_{1.25}Br_{1.75}$	2.44	0.14	81.9	3.2	7.81	3.3	0.76

Table S4. Summary of the device performance with $Rb_{0.33}Cs_{0.67}FA_{1.37}PbBr_3$ and $Rb_{0.33}Cs_{0.67}FA_{1.37}PbCl_{1.25}Br_{1.75}$ QDs as the light-emitting layers.

light-emitting layer	V_{on} [a] (V)	CE_{max} (cd/A)	EQE_{max} (%)	L_{max} (cd/m^2)	Peak (nm)	CIE [b] (x, y)
$(Rb_{0.33}Cs_{0.67})_{0.42}FA_{0.58}PbBr_3$	4.4	8.5	3.6	750	502	(0.08, 0.52)
$(Rb_{0.33}Cs_{0.67})_{0.42}FA_{0.58}PbCl_{1.25}Br_{1.75}$	4.0	0.45	0.61	39	466	(0.14, 0.07)
$Cs_{0.5}FA_{0.5}PbCl_{1.25}Br_{1.75}$	4.0	0.37	0.41	27	478	(0.16, 0.11)

[a] at the luminance of 1 cd/m^2.

[b] at the current density of 10 mA/cm^2.

References

1 J. Xing, Y. Zhao, M. Askerka, L. N. Quan, X. Gong, W. Zhao, J. Zhao, H. Tan, G. Long, L. Gao, Z. Yang, O. Voznyy, J. Tang, Z.-H. Lu, Q. Xiong, E. H. Sargent, *Nat. Commun.,* 2018, **9**, 3541.
2 Y. Wu, C. Wei, X. Li, Y. Li, S. Qiu, W. Shen, B. Cai, Z. Sun, D. Yang, Z. Deng, H. Zeng, *ACS Energy Lett.*, 2018, **3**, 2030.
3 H. Hu, L. Wu, Y. Tan, Q. Zhong, M. Chen, Y. Qiu, D. Yang, B. Sun, Q. Zhang, Y. Yin, *J. Am. Chem. Soc.*, 2018, **140**, 406.
4 Q. Zhang, R. Su, X. Liu, J. Xing, T. C. Sum, Q. Xiong, *Adv. Funct. Mater.*, 2016, **26**, 6238.
Z. Li, L. Kong, S. Huang, L. Li, *Angew. Chem. Int. Ed.*, 2017, **129**, 8246.

